

Effects of KF and RbF treatments on Cu(In,Ga)Se₂-based solar cells: A combined photoelectron spectroscopy and DFT study

I. Majumdar^{1,2,a)}, S. K. Sahoo^{3,b)}, V. Parvan^{1,4}, H. Mirhosseini³, B. Chacko¹, Y. Wang¹, D. Greiner^{1,5}, T. D. Kühne³, R. Schlatmann¹, I. Lauermann¹

¹*PVcomB/Helmholtz-Zentrum Berlin für Materialien und Energie, Schwarzschildstraße 3, 12489 Berlin, Germany*

²*Freie Universität Berlin, Fachbereich Physik, Arnimallee 14, 14195 Berlin, Germany*

³*Dynamics of Condensed Matter and Center for Sustainable Systems Design, Chair of Theoretical Chemistry, University of Paderborn, Warburger Straße 100, D-33098 Paderborn, Germany*

⁴*Present address: Feinmetall GmbH, Zeppelinstraße 8, 71083 Herrenberg, Germany*

⁵*Present address: Busch Produktions GmbH, Schauinslandstraße 1, 79689 Maulburg, Germany*

Abstract

In this work, the alkali-induced chemical and electronic modifications observed at the KF- and RbF-treated Cu(In,Ga)Se₂ (CIGSe)/CdS interfaces are correlated to a Density Functional Theoretical (DFT) model of the alkali metal induced point defects at a CuInSe₂/CdS interface. Analysed with hard X-ray photoelectron spectroscopy (HAXPES), the *near-interface* regions showed a Cu-poor, In-rich and stoichiometric CdS composition for the KF-CIGSe/CdS interface and a Cu-poor, In, S-rich composition for the RbF-CIGSe/CdS interface. The DFT-calculated defect formation energies and valence band offsets (VBO) at the defect-induced interfaces indicate towards possible formation of specific defects at the KF- and RbF-treated CIGSe/CdS interfaces. Cu vacancies indicated by the Cu-poor stoichiometry of the alkali-treated interfaces contribute to an increase in the acceptor densities (N_A). Possible formation of K_{Cu} and Rb_{Cu} defects could result in lower N_A at the interfaces because of the Cu vacancies being filled up by K and Rb atoms. Na_{Cd} and excess Cd_{Cu} defects at the KF-CIGSe/CdS interface and only Cd_{Cu} defects at the RbF-CIGSe/CdS interface might have formed that would result in higher donor densities (N_D) at the interfaces. These factors, which showed enhanced type-inversion when applied in device simulations, resulted in fill factor (FF) and open-circuit voltage (V_{oc}) gains in devices.

Keywords: Cu(In,Ga)Se₂, Alkali treatment, Hard X-ray Photoelectron Spectroscopy, Absorber/Buffer interface

^{a)}Email: isheta.majumdar.iitb@gmail.com

^{b)}Email: sahuo@campus.uni-paderborn.de

1. Introduction

Cu(In,Ga)Se₂ (CIGSe) has attracted large interest in the scientific community owing to its applications in the most efficient thin-film solar cells [1, 2]. It has been reported that the presence of the alkali metal atoms in the CIGSe absorber increases the efficiency of solar cells [3-5]. This increase in efficiencies has been a result of treatment of CIGSe with alkali fluorides like sodium fluoride (NaF), potassium fluoride (KF), and rubidium fluoride (RbF). The major influence is on the open-circuit voltage (V_{oc}) and the fill factor (FF) of the solar cells. It is crucial to find the reason behind such an increase in these cell parameters and also the limiting factors involved as sometimes alkali-treatment also led to drop in FF [6, 7]. The answer to this lies in the dynamics of the alkali-treated absorber (CIGSe) / cadmium sulphide (CdS) buffer layer heterojunction region as well as in the alkali-treated absorber *near-surface* and *near-bulk* regions. In 2018, the then record lab cell efficiency (22.6% [8]) of CIGSe-based thin film solar cells was achieved by a post deposition treatment (PDT) with RbF (alkaline treatment after completion of CIGSe growth, in Se atmosphere). The present world record lab cell efficiency stands at 23.3% [9] also due to alkali treatment (CsF-PDT).

The mechanisms that lead to the enhancement of the cell performance could be categorized in two groups: (i) the enhancement of the carrier concentration, and (ii) the enhancement of the carrier lifetime. While the former is related to the absorber layer, the latter has to do with the grain boundaries and interfaces. Most of the theoretical studies done so far reported that the most stable alkali metal defects in CIGSe are either electrically neutral (Cu-substitutional defects) or detrimental to hole conductivity (interstitial defects) [10, 11]. On the other hand, the enhancement of the cell performance could be due to the modifications of the electronic structure of the interfaces in a cell, i.e. at the front contact CIGSe/CdS interface and/or at the back contact CIGSe/Mo interface. The band-alignment and the band offsets of the heterostructures are crucial for the transfer of photo-generated carriers across the interfaces. There are a few studies on the CIGSe/CdS heterostructure in terms of both theory [12-14] and experiments [15-25], but none correlating the two aspects. The fact that alkali metal deposition affects the chemical composition of the CIGSe absorber and thus “conditions” or passivates the surface for better alignment with the subsequent buffer layer deposition has been shown by previous experimental investigations [3, 4, 26, 27], but not in the nanometer scale.

He et al. [28] have shown the presence of Cd atoms incorporated in the CIGSe matrix and Cu atoms in CdS, confirming the exchange of Cd and Cu in the CIGSe/CdS heterostructure. Such intermixing of atoms at the CIGSe/CdS heterostructure can change the band gap of the absorber and band-offsets at the interface. Optimum band alignment (conduction and valence bands) of the heterojunction and proper band offset at the absorber/buffer interfaces are crucial for the collection of photo-generated carriers. In spite of their paramount importance, there has not been any systematic study about the effect of various alkali-metal induced point defects on the band alignment at the CIGSe/CdS heterojunction. Therefore, this work focusses on a systematic study of the chemical and electronic modifications associated with KF and RbF treatments (presented in Section 3.1) as well as the impact on the CIGSe/CdS heterojunctions (presented in Sections 3.3 and 3.4) as a result of both PDTs. Density functional theory (DFT) [29] based calculations were performed to study the formation energies of various alkali metals-related point defects and the band-alignment of the CuInSe₂ (CISe)/CdS interface heterostructures in the presence of these alkali metals-related point defects. These results (presented in Section 3.2) have been used to interpret the X-ray spectroscopic observations. X-ray photoelectron spectroscopy (XPS) data, in general, give information in the nanometer range that makes these data more comparable to the theoretical investigations. Based on the possible effects of the presence of the alkali metal induced point defects at the CIGSe/CdS interface as well as the chemical changes observed in the absorbers spectroscopically, approximate models of the alkali incorporation have been suggested for the KF and RbF treatments in CIGSe. Based on these models, device simulations have been performed, using the 1-D numerical simulation software Solar Cell Capacitance Simulator (SCAPS) (presented in Section 3.5), to reproduce the trends in the deviation of the cell parameters of the real devices made from KF-treated and RbF-treated CIGSe absorbers in comparison to a reference device made from an untreated CIGSe absorber. The device simulations help in validating the plausibility of the presently suggested models of alkali incorporation in CIGSe.

2. Material and methods

2.1 Cu(In,Ga)Se₂ absorber preparation

All the CIGSe absorber materials used in this study were prepared at the PVcomB labs by growing CIGSe on Mo-coated soda lime glass (SLG) substrates using a multisource (Cu, In, Ga, Se) three-stage physical vapor deposition (PVD) co-evaporation process [30, 31]. A schematic diagram of the process is depicted in Figure S1 (SI 1). It shows the rate of metal deposition on the upper panel and the substrate temperature in the lower panel at various stages of deposition. In the first stage, a sequential deposition of In-Se and Ga-Se precursor layers was done at a nominal substrate temperature of $T_1 \sim 620$ K (347 °C). In the second stage,

In and Ga fluxes were turned off and only Cu and Se were offered to the substrate at a nominal temperature of $T_2 \sim 800$ K (527 °C). In the final stage, In and Ga fluxes were reopened (In-Ga-Se deposition) and the Cu flux was turned down. This resulted in the deposition of CIGSe layers with Cu-poor composition. For the present study, CIGSe absorbers of nominal bulk $[Cu]/([Ga]+[In])$ (CGI) ratios in the range 0.85-0.95 were prepared. The deposition chamber consists of a laser for in-situ process control. Before alkali treatment, all CIGSe absorbers used for investigation were etched with 5% KCN (potassium cyanide) solution for three minutes, then washed with de-ionized water, followed by drying with a nitrogen stream.

2.2 Alkali fluoride deposition from effusion cell

In our standard effusion cells, the evaporant in the crucible is heated by tantalum wire filaments. An operation temperature stability of ± 0.1 K by proportional-integral-derivative (PID) control enables very stable and reproducible growth rates in an extremely wide range from below 1 Å/min for doping applications up to several nm/min for thin film growth [32]. For the current experiments, a thermocouple was kept fixed near the bottom of the crucible for temperature observations. The parameters for various alkali fluoride depositions done in this work are shown in Table S1 (SI 2). The alkali fluoride deposition was followed by annealing of the samples at 350 °C for 10 minutes. It should be noted that the alkali treatment done in this work is different from the conventional PDT method used by others, as (i) alkali fluoride deposition was done in an ultra-high vacuum (UHV) chamber, (ii) at room temperature, (iii) a further annealing step after alkali fluoride deposition, and (iv) there was no external Se supply during the alkali fluoride deposition.

2.3 Chemical bath deposition (CBD) of CdS

CdS deposition by the CBD method consists of release of Cd^{2+} and S^{2-} ions in an aqueous solution and subsequent deposition on an immersed substrate, in this case, CIGSe. For this purpose, 1.06 g of cadmium acetate dehydrate ($Cd(CH_3CO_2)_2 \cdot 2H_2O$) was dissolved in 20 ml of distilled water (Cd^{2+} ion source) and 6.1 g of thiourea ($SC(NH_2)_2$) was dissolved in 100 ml of distilled water (S^{2-} ion source). Next, 16.25 ml of ammonia (NH_3) solution (25%) was added to 125 ml of distilled water in the presence of a magnetic stirrer in a double glass-walled 200 ml beaker with warm water flowing in the cavity of the double walls (chemical bath). After this, 2.5 ml of the Cd acetate solution and 12.5 ml of the thiourea solution were added to the chemical bath which was then filled up to 200 ml with distilled water. After reaching 46 °C in the chemical bath, the samples were inserted into the CBD solution for ~ 50 s in order to deposit very thin CdS layers of ~ 5 -10 nm.

2.4 Hard X-ray photoelectron spectroscopy (HAXPES) measurements

HAXPES measurements with varying X-ray energies were done at the HIKE beamline [33, 34] for excitation energies ($h\nu$) 2030, 3000, 4000, 5000 and 6000 eVs. The high kinetic energy (HIKE) end-station at the KMC-1 beamline of BESSY II is a system designed for hard X-ray photoelectron spectroscopy (HAXPES) measurements in samples to probe the *near-surface* and *near-bulk* of materials and buried interfaces under incident X-ray excitation energies in the range of 2-12 keV. The KMC-1 beamline uses a double crystal monochromator using different sets of crystals. In this study, all measurements were done using the Si (111) crystal resulting in a beamline resolution of ~ 0.2 eV at 2030 eV photon energy and ~ 1.2 eV at 6000 eV [33]. Quantitative analysis of the XPS measurements was done by converting the raw HAXPES data into normalized peak intensities by dividing the measured peak areas by the following factors: the number of scans (N), the IMFP (λ) of ejected photoelectrons which is a measure of the average distance travelled by an electron beam through a material before it loses energy through inelastic scattering and its intensity is reduced to a fraction of $1/e$ of the initial intensity, the photoionization cross-sections of emitted photoelectrons (σ) [35] and the transmission function of the spectrometer (T). The experimentally obtained HAXPES intensities after normalization have been fitted with a bi-layer model equation (Eq. 5 in SI 4) to obtain *near-surface* and *near-bulk* atomic concentration values. In the case of CIGSe/CdS interface investigations (later in Section 3.3), *near-interface* and *near-bulk* atomic concentration values have been obtained using the same bi-layer model fitting equation.

The types of samples investigated are: (i) bare CIGSe absorber, (ii) KF-treated CIGSe absorber (KF-CIGSe), (iii) RbF-treated CIGSe absorber (RbF-CIGSe), (iv) CIGSe absorber with thin CdS deposition (CIGSe/CdS), (v) KF-treated CIGSe absorber with thin CdS layer deposition (KF-CIGSe/CdS), and (vi) RbF-treated CIGSe absorber with thin CdS layer deposition (RbF-CIGSe/CdS).

2.5 Density Functional Theory (DFT)-based simulations of alkali metal (AM) point defects at a model CIGSe/CdS heterostructure

The point defects due to AM atoms in a theoretical CIGSe/CdS interface heterostructure are modelled by employing DFT based calculations. The details of DFT calculations and the heterostructure model are given in SI 3. The CIGSe/CdS heterostructure model considered in this study is a perfect system with no defects in the CIGSe and CdS bulk, except at the CIGSe/CdS interface. The CIGSe/CdS heterostructure model was constructed from CIGSe (110) surface and CdS (110) surface. The surface atoms are tri-coordinated in both CIGSe (110) and CdS (110) surfaces. In the CIGSe/CdS heterostructure, at the interface, all these tri-coordinated atoms form another covalent bond upon relaxation (see Figure S2). The Cu and the In atoms of CIGSe (110) surface at the interface coordinated to three Se atoms, now forms a bond with tri-coordinated

S atoms of CdS. Similarly, the tri-coordinated Se atoms at the interface form covalent bond with a tri-coordinated Cd atom.

In order to study the AM defect, one AM atom is introduced in the first atomic layer at the interface of the heterostructure either as a substitutional defect (by replacing one of the constituent atoms from the lattice) or as an interstitial defect. The AM atom is covalently bonded with three Se atoms of CISE and one S atom of CdS when it replaces either Cu or In atom at the interface. Whereas, the AM atom is bonded to three S atom and one Se atom when it replaces one Cd atom (see Figures S3-S5).

The band alignment and the band offset for the CISE/CdS heterostructure have been calculated by employing a hybrid DFT functional (HSE06) with and without defects using the average electrostatic method [36]. In this method, the valence band offset (VBO) is calculated as:

$$\text{VBO} = \Delta E_V + \Delta V \quad (1)$$

where, ΔE_V is the difference between the valence band maxima (VBM) of the valence bands of bulk CISE and CdS, and ΔV represents the average macroscopic potential difference across the interface in the CISE/CdS heterostructure. In order to compute the conduction band offset (CBO) the experimental band gap of the corresponding material is taken into account.

2.6 Solar cell device preparation and characterization

Solar cell devices were completed from the absorbers with a 60 nm CdS chemical bath deposition, followed by 40 nm i-ZnO/110 nm ZnO:Al deposition and Ni/Al/Ni front contact grids with 1 cm² active areas. Current density-voltage (J-V) measurements of the devices were performed under an AM 1.5G illumination (100 mW cm⁻²) sun simulator, calibrated using a reference Si cell, using a four-point-probe Keithley 2601A source measure unit.

3. Results and discussion

3.1 Chemical and electronic effects of KF and RbF treatments on Cu(In,Ga)Se₂ absorber surfaces

The effect of alkali treatment on the *near-surface* and *near-bulk* regions of the untreated and alkali-treated CIGSe absorbers have been investigated using HAXPES data in conjunction with a bi-layer model discussed in SI 4. The chemical compositions of the alkali-treated CIGSe absorbers in terms of the percentage atomic concentrations of the constituent elements have been calculated (shown in SI 5). Because each sample is different, the depths of the *near-surface* regions obtained from the bi-layer model for each

sample are different. As per the bi-layer model, the KF-CIGSe absorber (Figure S7 (a)) forms a *near-surface* region of thickness 35 ± 3 nm and composition $\text{Cu}_{0.8}(\text{In,Ga})_{3.4}\text{Se}_{2.0}$, which is equivalent to the ordered defect compound (ODC) composition (Cu-poor, In, Ga-rich); while the RbF-CIGSe absorber (Figure S7 (b)) forms a highly Cu-poor *near-surface* region of thickness 24 ± 3 nm and composition $\text{Cu}_{0.3}(\text{In,Ga})\text{Se}_{2.0}$. The *near-bulk* layers of both alkali-treated CIGSe absorbers are Cu, In, Ga-rich with compositions $\text{Cu}_{1.1}(\text{In,Ga})_{2.8}\text{Se}_{2.0}$ and $\text{Cu}_{1.7}(\text{In,Ga})_{3.7}\text{Se}_{2.0}$ for the KF-CIGSe and RbF-CIGSe absorbers, respectively.

In order to further investigate the chemical modifications seen in the *near-surface* regions of the alkali-treated CIGSe absorbers, it is of interest to look for any surface modifications at the very surface of the absorbers. Therefore, in this section, the surface regions of the untreated CIGSe, the KF-CIGSe and the RbF-CIGSe absorbers have been studied, which can shed some light on the differences or similarities between the two types of alkali treatment. The Na $1s_{1/2}$ component of KF-CIGSe (Figure S8 in SI 6) has a much higher peak intensity (~ 4 times) as compared to the Na $1s_{1/2}$ peaks in CIGSe and RbF-CIGSe, indicating a higher Na concentration at the KF-CIGSe surface.

As per the modified Auger parameter values (α') calculated (Table S2 in SI 6), there are significant differences in the α' values in Ga and In components of the different samples. The fitted components of the In $3d_{5/2}$ photoelectron and In $M_{4,5}N_{45}N_{45}$ Auger lines measured with a Mg $K\alpha$ source are shown in Figures 1 (a) and (b), respectively. It can be seen that the In $3d_{5/2}$ spectra of both KF-CIGSe and RbF-CIGSe show two clear peak components marked by (I) and (II). In both cases, two corresponding Auger peak components are also seen in their respective In $M_{4,5}N_{45}N_{45}$ spectra marked by (a) and (b) associated with the photoelectron peak components (I) and (II), respectively. The In $M_{4,5}N_{45}N_{45}$ spectra in KF-CIGSe (middle panel of Figure 1 (b)) and RbF-CIGSe (bottom panel of Figure 1 (b)) have been fitted with the overall In $M_{4,5}N_{45}N_{45}$ spectra envelope of the reference CIGSe sample (top panel of Figure 1 (b)).

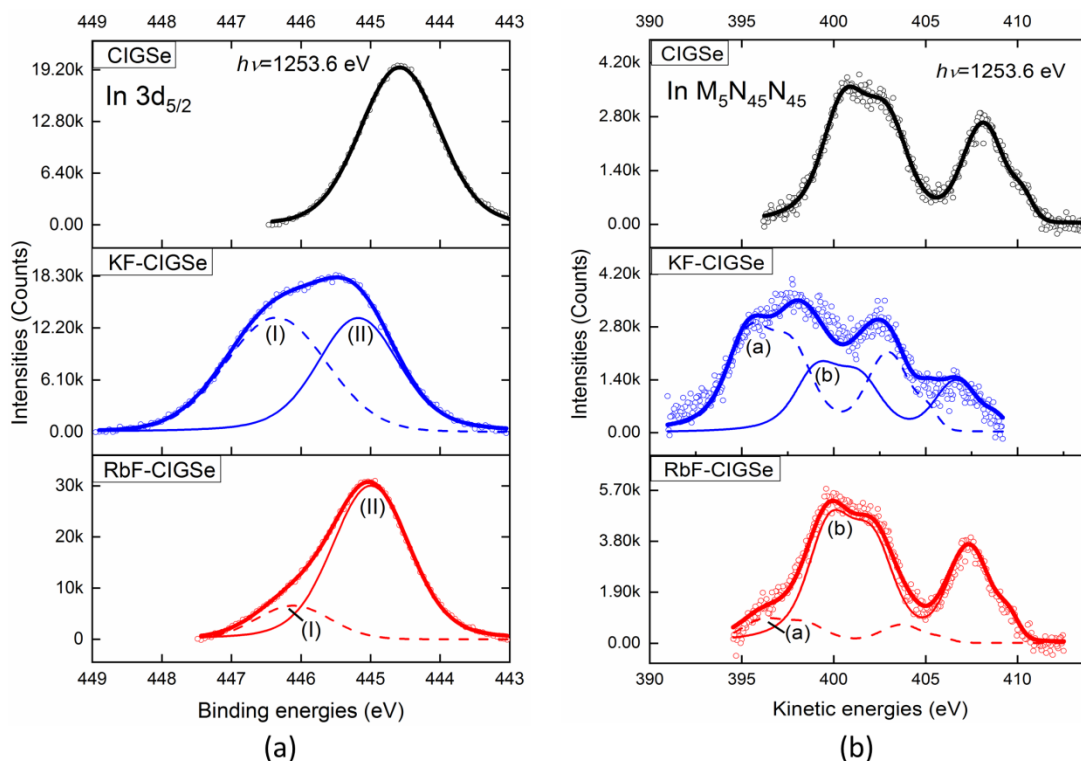


Figure 1 (color online) (a) In $3d_{5/2}$ (b) In $M_{4,5}N_{45}N_{45}$ Auger peak components in CIGSe, KF-CIGSe and RbF-CIGSe measured with a lab-based Mg K_{α} XPS source.

From the Wagner plot of In (Figure 2), the two types of In components in KF-CIGSe are: KF-CIGSe (Ia) and KF-CIGSe (Iib), while in RbF-CIGSe, these are: RbF-CIGSe (Ia) and RbF-CIGSe (Iib). While the CIGSe component of In lies close to compounds like InSe and In_2Se_3 , the components KF-CIGSe (Iib) and RbF-CIGSe (Iib) of In lie close to In_2O_3 and thus indicate formation of In-O bonds at both KF-CIGSe and RbF-CIGSe surfaces. On the other hand, the RbF-CIGSe (Ia) component directly indicates the formation of InF_3 while the KF-CIGSe (Ia) component lies along the line containing the compound $(NH_4)_3InF_6$, thus indicating formation of In-F bonds at both KF-CIGSe and RbF-CIGSe surfaces. However, the quantity of In-F formation seems to be higher at the KF-CIGSe surface than at the RbF-CIGSe surface.

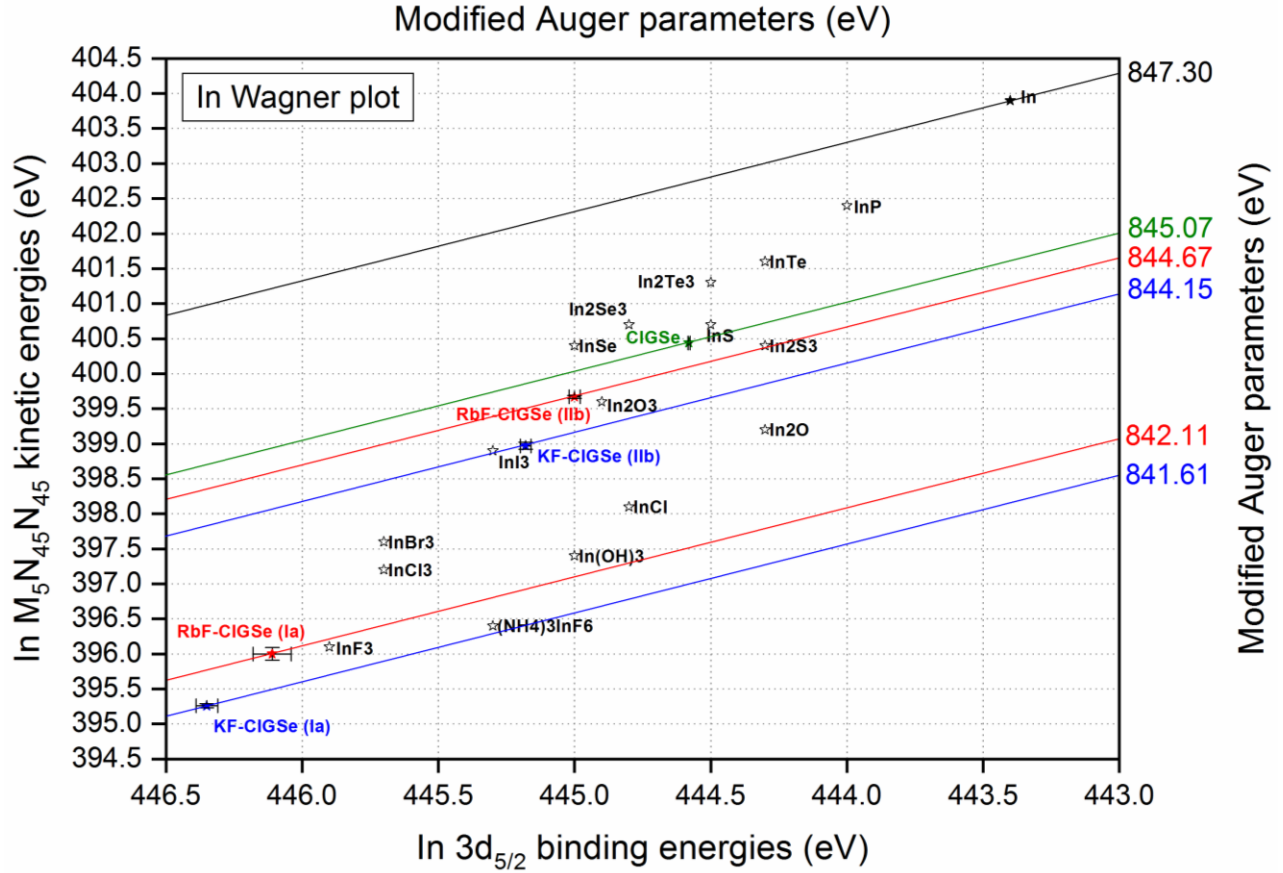


Figure 2 (color online) Wagner plot for indium. Core-level BE, Auger line KE values of compounds from literature (black) were taken from [37].

Figure 3 shows the Ga $2p_{3/2}$ fit components for the untreated and alkali-treated CIGSe absorbers at $h\nu=2030$ eV. It can be seen that a second Ga $2p_{3/2}$ component (dashed curve) shows up in both KF-CIGSe and RbF-CIGSe besides the Ga $2p_{3/2}$ component of untreated CIGSe. This could indicate the formation of a Ga_2O_3 layer [38] but the formation of an oxide on the alkali-treated CIGSe absorbers seems less likely because the binding energy of the observed additional peak after alkali fluoride treatment is consistent with Ga-F. The fact that this extra Ga component that shows up for both alkali-treated CIGSe absorbers is on the higher binding energy side, rules out the possibility of the formation of metallic Ga.

We also measured F peaks. For both alkali treatments, they lie at the binding energy positions of 685 eV. Since the F peaks from the KF and RbF are huge, the In-F/Ga-F peak components may be significantly smaller and hence not resolvable.

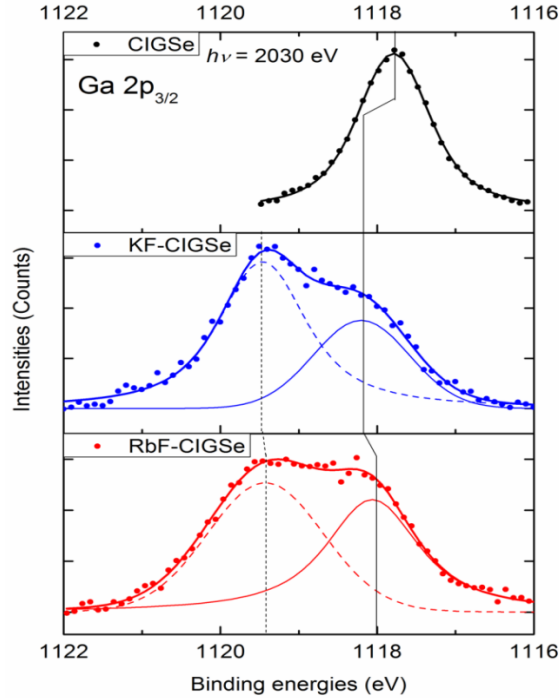


Figure 3 (color online) Ga $2p_{3/2}$ HAXPES peak components from 2030 eV excitation energy. Ga-F formation is indicated by the appearance of an extra Ga $2p_{3/2}$ component (dashed curves) on the higher BE side of the spectra in the case of the alkali-treated CIGSe surface regions.

Finally, we examined the impact of the alkali treatment on the electronic structure of the CIGSe absorber surface as well as the absorber/buffer interface. Figure 4 shows the VBM values of the untreated and alkali-treated CIGSe absorber surfaces obtained from lab-based surface-sensitive ultra-violet photoelectron spectroscopy (UPS) measurements ($h\nu=21.22$ eV). The VBM positions obtained are 0.47 ± 0.06 eV, 2.03 ± 0.12 eV and 1.39 ± 0.14 eV w.r.t. the Fermi level position, for the bare CIGSe, KF-CIGSe and RbF-CIGSe absorbers, respectively. It can be clearly observed that the alkali-treated CIGSe absorbers have much higher VBM values than the untreated one. This could indicate the presence of alkali-related secondary phases at the absorber surface [10]. Some of the theoretically suggested secondary phases that can form on CIGSe absorber surfaces are $KInSe_2$, $K_{12}In_2Se_9$, K_9InSe_7 , KSe and K_2Se_3 for KF-CIGSe absorbers and $RbInSe_2$, $RbCuSe_4$, $RbSe$, Rb_2Se_3 and Rb_2Se_5 for RbF-CIGSe absorbers, all of which have similar band gap values as presently observed (>2 eV) [10]. Both K-related [39] and Rb-related [40] secondary phases have been found to be n-type.

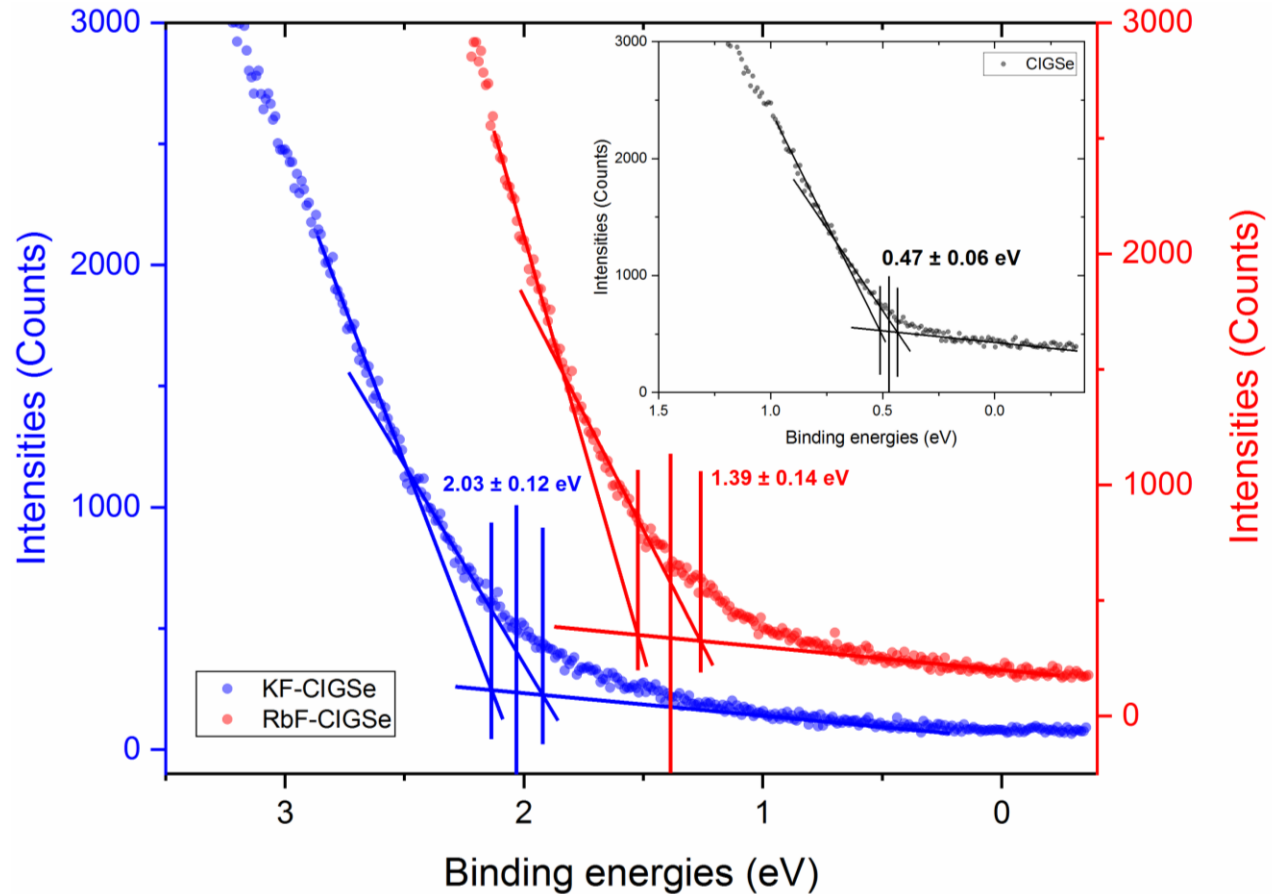


Figure 4 (color online) VBM values of CIGSe absorber surfaces measured with lab-based He I source (UPS). Here, the point midway between the two extreme inflexion points have been considered as the measured VBM positions and the total uncertainty is the difference between the two inflexion point positions.

3.2 Alkali metal (AM) point defect formation at the $\text{CuInSe}_2/\text{CdS}$ heterostructure: DFT results

The defect formation energies of various point defects at the $\text{CuInSe}_2/\text{CdS}$ heterostructure are listed in Table 1. It can be seen that for substitutional defects, AM atoms prefer the Cu lattice compared to In and Cd lattices, which is consistent with the previous results for the bulk CuInSe_2 [10, 11]. AM atoms can also form interstitial defects, owing to their corresponding low formation energies. Moreover, it is to be noted that the formation energies increase with increasing size of the AM atoms.

It is widely accepted that the nature of the $\text{CuInSe}_2/\text{CdS}$ heterostructure is partially intermixed rather than having a defined interface [15,17,22]. This is due to the exchange of the respective atoms from the absorber and buffer layers. In order to have a more realistic picture, we considered two types of the atom exchange:

cations exchange ($\text{Cd} \leftrightarrow \text{Cu}$ and $\text{Cd} \leftrightarrow \text{In}$) and anion exchange ($\text{S} \leftrightarrow \text{Se}$); see Figure S6. The corresponding defect formation energies (Table 1) suggest that the anion exchange is more preferred than the cation exchange. Park et al. [20] have reported the intermixing of Cd and Cu at the interface. The low formation energy for the Cd-Cu intermixing (see Table 1) from our calculation supports this data. As the defect formation energy given in Table 1 shows that the AM_{Cu} defects are most likely to form at the interface, therefore, we also study these defects in combination with the intermixing of atoms at the interface. However, interestingly, we notice that the change in total formation energy due to both of these defects (intermixing + AM_{Cu}) is marginal, which confirms these defects do not interact with each other.

The list of VBO and CBO with various AM-related defects in the heterostructure is given in Table 1. It can be seen that the defect-free CISE/CdS interface is a Type I or “spike-like” heterojunction. This means that the conduction band minimum (CBM) is higher on the CdS side, which is in agreement with previous findings [12, 13]. The VBO and the CBO of the CISE/CdS interface without any defects are found to be 1.09 eV and 0.28 eV, respectively. It is to be noted that for the calculation of CBO, experimental band gaps of CISE (1.04 eV) and CdS (2.42 eV) were taken into account. Our DFT results suggest that the VBO decreases and the CBO increases in the presence of AM substitutional defects. Among all the substitutional defects, when a Cu atom is replaced by an AM atom (AM_{Cu}), the changes in both the VBO and the CBO are marginal. However, the presence of AM_{In} and AM_{Cd} defects increase the CBO to values greater than 0.5 eV, which usually results in a poor device performance. On the other hand, the presence of interstitial defects increases the VBO and reduces the CBO down to near-zero values (flat CB alignment), which is often considered as a good working heterojunction.

The exchange of atoms due to intermixing at the interface also influences the band offset values. Based on our calculations, $\text{Cd} \leftrightarrow \text{Cu}$ exchange results in reduced VBO and enhanced CBO. However, both $\text{Cd} \leftrightarrow \text{In}$ and $\text{S} \leftrightarrow \text{Se}$ exchange result in enhanced VBOs and negative CBOs, i.e. Type II or “cliff-like” heterojunctions. Moreover, the presence of AM substitutional defects AM_{Cu} along with the intermixing does not affect the band offset values significantly.

Table 1 The defect formation energies, valence band offset (VBO) and conduction band offset (CBO) for various point defects at the CISE/CdS interface.

CuInSe₂/CdS	ΔE_f (eV)	Valence band offset (eV)	Conduction band offset (eV)
Defect-free		1.09	0.28
Na _{Cu}	-0.85	1.06	0.31
K _{Cu}	-0.05	1.04	0.33
Rb _{Cu}	0.35	1.01	0.36
Na _{int}	-0.66	1.31	0.06
K _{int}	0.41	1.31	0.06
Na _{In}	0.64	0.81	0.56
K _{In}	1.25	0.83	0.54
Rb _{In}	1.60	0.83	0.54
Na _{Cd}	-0.09	0.69	0.68
K _{Cd}	0.55	0.73	0.64
Rb _{Cd}	0.93	0.74	0.63
Cd-Cu mixing	0.55	0.57	0.80
(Cd-Cu mixing)+Na _{Cu}	-0.35		
(Cd-Cu mixing)+K _{Cu}	0.33		
(Cd-Cu mixing)+Rb _{Cu}	0.71		
Cd-In mixing	0.47	1.53	-0.15
(Cd-In mixing)+Na _{Cu}	-0.39		
(Cd-In mixing)+K _{Cu}	0.38		
(Cd-In mixing)+Rb _{Cu}	0.79		
S-Se mixing	0.05	1.10	-0.43
(S-Se mixing)+Na _{Cu}	-0.86		
(S-Se mixing)+K _{Cu}	-0.05		
(S-Se mixing)+Rb _{Cu}	0.43		

3.3 Chemical effects of KF and RbF treatments at Cu(In,Ga)Se₂/CdS interfaces

In order to observe any chemical modifications after CdS deposition and possible exchange of absorber and buffer atoms across the interface, in this section, the effect of alkali treatment on the *near-interface* and *near-bulk* regions of the untreated and alkali-treated CIGSe/CdS interfaces have been investigated using HAXPES data in conjunction with the bi-layer model discussed in SI 4. Figures 5 (a), (b) and (c) show the chemical compositions of the untreated CIGSe/CdS interface, the KF-CIGSe/CdS interface and the RbF-CIGSe/CdS interface, respectively.

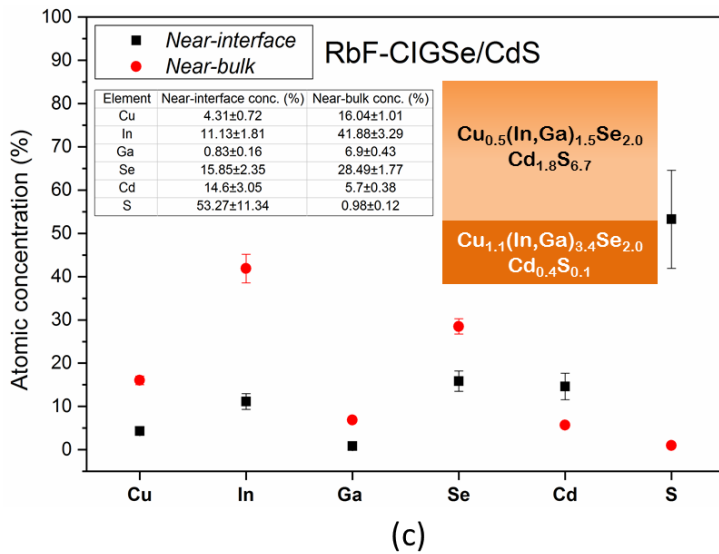
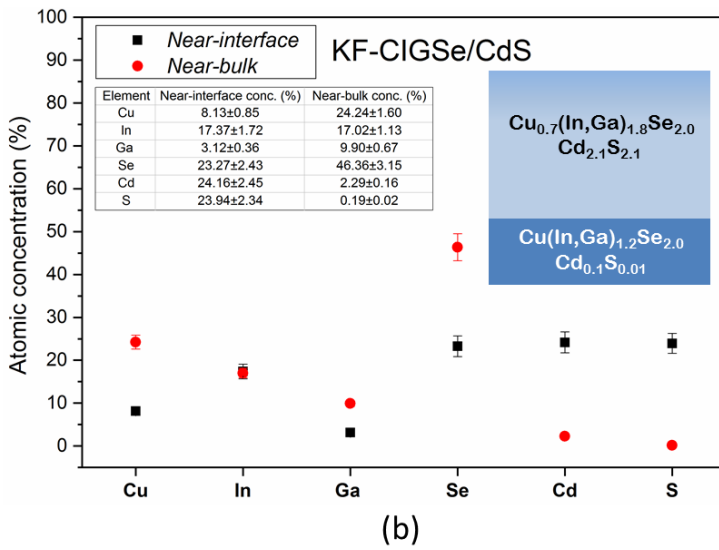
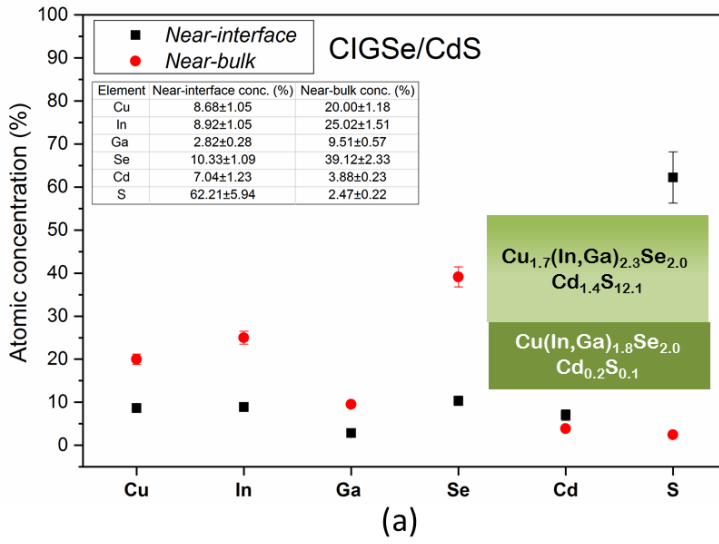


Figure 5 (color online) *Near-interface* and *near-bulk* chemical compositions of (a) CIGSe/CdS (b) KF-CIGSe/CdS and (c) RbF-CIGSe/CdS interfaces.

A Cu, In-rich *near-interface* region of thickness 24 ± 3 nm and composition $\text{Cu}_{1.7}(\text{In,Ga})_{2.3}\text{Se}_{2.0}$ and an In-rich *near-bulk* region of composition $\text{Cu}(\text{In,Ga})_{1.8}\text{Se}_{2.0}$, is observed for the untreated CIGSe/CdS interface (Figure 5 (a)). Among the alkali-treated absorbers, the KF-CIGSe/CdS interface (Figure 5 (b)) forms a Cu-poor, In-rich *near-interface* region of thickness 30 ± 3 nm and composition $\text{Cu}_{0.7}(\text{In,Ga})_{1.8}\text{Se}_{2.0}$; while the RbF-CIGSe/CdS interface (Figure 5 (c)) also forms a Cu-poor, In-rich *near-interface* region of thickness 20 ± 3 nm and composition $\text{Cu}_{0.5}(\text{In,Ga})_{1.5}\text{Se}_{2.0}$. The *near-bulk* region of the KF-CIGSe/CdS interface has been found to be In-rich with a composition of $\text{Cu}(\text{In,Ga})_{1.2}\text{Se}_{2.0}$, while the *near-bulk* region of the RbF-CIGSe/CdS interface has been found to be Cu, In-rich with a composition of $\text{Cu}_{1.1}(\text{In,Ga})_{3.4}\text{Se}_{2.0}$. As for the buffer-related elements, the *near-interface* region of the untreated CIGSe/CdS interface has a highly S-rich composition. For the KF-CIGSe/CdS interface, the *near-interface* region has a stoichiometric CdS composition, while for the RbF-CIGSe/CdS interface; the *near-interface* region has a S-rich composition. This also indicates deposition of non-stoichiometric CdS [22]. The CGI ratios (Figure 6) indicate that while the RbF-CIGSe/CdS interface is Cu-poor throughout, the *near-bulk* region of the KF-CIGSe/CdS interface is slightly Cu-rich.

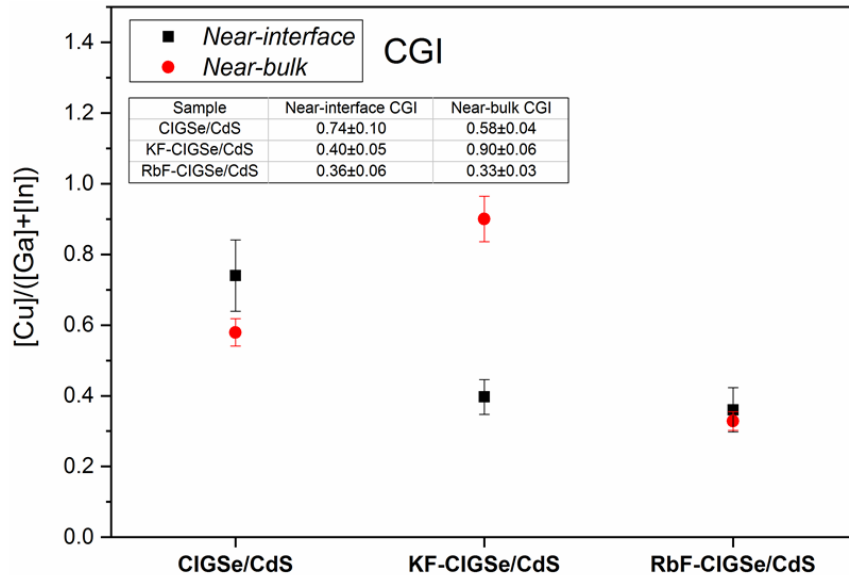


Figure 6 (color online) CGI ratios of untreated and alkali-treated CIGSe/CdS interfaces.

The exchange between S atoms of the CdS buffer overlayer and Se atoms of the CIGSe absorber substrate layer at the KF-CIGSe/CdS interface as compared to the untreated CIGSe/CdS interface is evident from the $[\text{S}]/([\text{Se}]+[\text{S}])$ ratios of Figure 7. The smaller difference between the *near-interface* and *near-bulk* $[\text{S}]/([\text{Se}]+[\text{S}])$ ratios indicate higher $\text{S}\leftrightarrow\text{Se}$ exchange at the KF-CIGSe/CdS interface. Considering the error bars, the extent of S-Se intermixing at the RbF-CIGSe/CdS interface is comparable to that at the untreated CIGSe/CdS interface. Based on DFT results given in Table 1, it can be seen that the S-Se

intermixing can occur more readily than the cation intermixing due to its low formation energy. In addition, in the presence of the S-Se intermixing, the formation energies of AM substitution defects are not greatly influenced. Thus, the S-Se intermixing may not determine the amount of AM substitution defects formed but rather influence the formation of absorber-buffer mixed secondary phases. So, it may be expected that the KF-CIGSe/CdS interface has these mixed phases consisting of the absorber and buffer-related elements, e.g. Cd(S,Se) [18] or CuIn(Se,S)₂ [41].

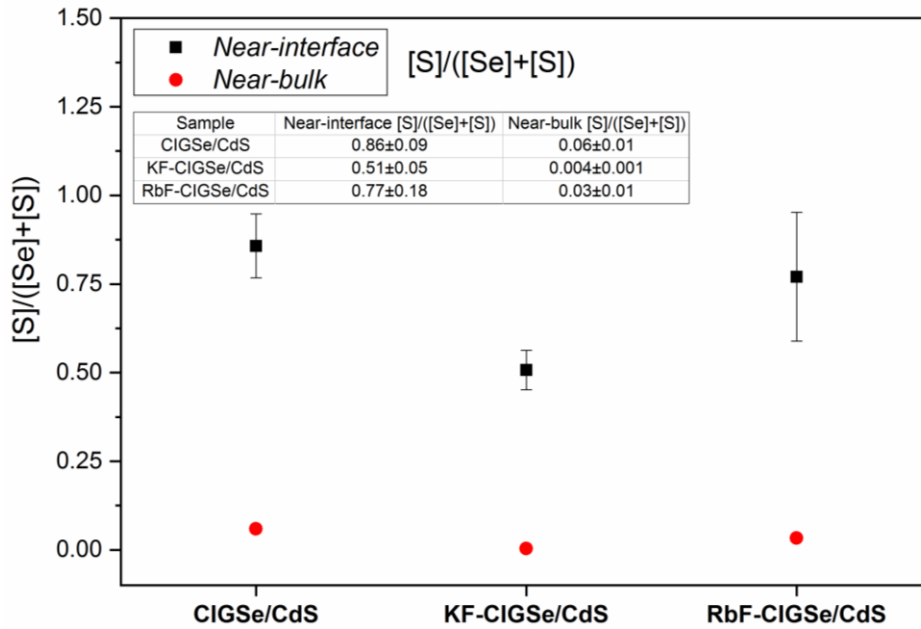


Figure 7 (color online) [S]/[Se] ratios of untreated CIGSe/CdS and alkali-treated CIGSe/CdS interfaces.

3.4 Electronic effects of KF and RbF treatments at Cu(In,Ga)Se₂/CdS interfaces

Here, we examined the impact of the alkali treatment on the electronic structure of the absorber/buffer interface. The VBM values shown in Figure 8 have been corrected by the interface-induced band-bending, which are changes in the BE positions of the CIGSe-related core-level HAXPES signals after CdS deposition and consequent interface formation (list of all core-level signal combinations shown in Tables S3, S4 and S5 in SI 7). The VBM measurements are shown in Figures S9, S10 and S11 in SI 8. From the VBM values, it can be seen that there has been an overall VBM shift away from the Fermi level for CIGSe in both alkali-treated CIGSe/CdS interfaces, considering the region from the *surface* to *near-bulk* investigated using HAXPES. The average VBM of CIGSe is +0.52 eV and +0.38 eV further away from the Fermi level at the KF-CIGSe/CdS and the RbF-CIGSe/CdS interfaces, respectively, in comparison to the average VBM position of CIGSe at the untreated CIGSe/CdS interface which is at +0.21 eV away from the Fermi level. This would mean, considering constant band edges for the complete CdS layer for all the

interfaces (untreated and alkali-treated), the VBOs at the alkali-treated CIGSe/CdS interfaces would be reduced by an amount equal to the downward shift in VBM compared to the VBO at the untreated CIGSe/CdS interface. According to the DFT results (see Table 1), a reduction in VBO is observed when Na_{Cu} , K_{Cu} , Rb_{Cu} , Na_{In} , K_{In} , Rb_{In} , Na_{Cd} , K_{Cd} and Rb_{Cd} substitutional defects form at the alkali-treated interfaces. However, from the defect formation energy calculations (Table 1), it can be seen that among the Na-related point defects, Na_{Cd} defect formation is the most favourable because of its high negative formation energy. Whereas for K and Rb, K_{Cu} and Rb_{Cu} defects formation, respectively, are the most favourable. According to calculations shown in Table 1, VBO reduction may also take place in the presence of Cd-Cu intermixing which could mean Cd_{Cu} defect formation.

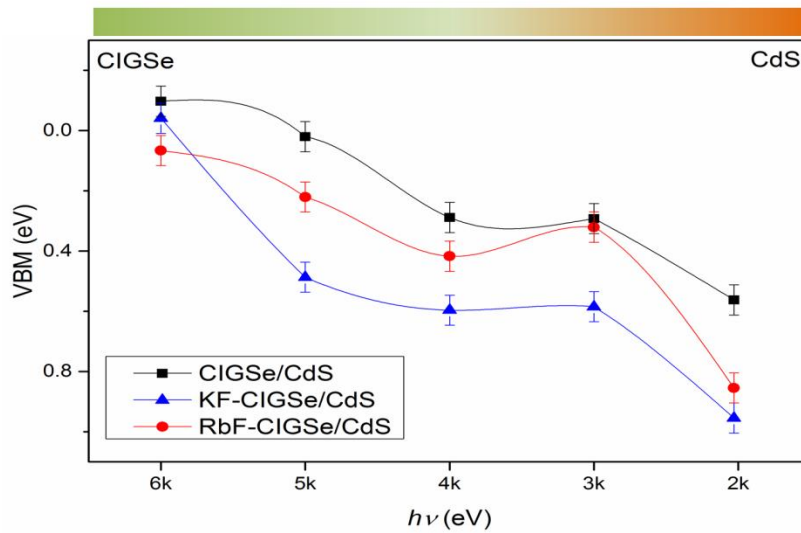


Figure 8 (color online) VBM values of CIGSe/CdS interface region measured with HAXPES with the interface-induced band-bending corrections taken into account. The lines connecting the data points are only a guide to the eye.

If bulk recombination is not dominating, then lowering of the VBM at the absorber/buffer interface would also indicate towards increased n-type doping that leads to slightly decreased V_{oc} since it depends on the effective hole density [42, 43] but increased FF for devices. This lowering of the VBM indicates an increase in the electron affinities (χ) of the alkali-treated CIGSe absorbers and is a direct evidence for type-inversion at the interface. Thus, there is greater type-inversion at the KF-CIGSe/CdS interface than at the RbF-CIGSe/CdS interface.

In terms of the effect of both alkali metal point defects and CIGSe-related point defects possibly formed due to the alkali treatment that were based on experimental observations, the following conclusions can be drawn:

(i) Although, AM_{Cu} defects are themselves neutral defects, but by filling up the Cu vacancies, the Cu vacancy defects (V_{Cu}) get reduced, which would mean reduced hole concentration [44]. Both KF-CIGSe and RbF-CIGSe absorbers have shown significant Ga-F, In-O and In-F formation as seen from the chemical changes at the absorber surfaces (Section 3.1). Both In-F and Ga-F salts are soluble in ammonia [45]. This indicates that In-F and Ga-F compounds may have dissolved in the CdS buffer layer (that contains ammonia solution) and led to In- and Ga-reduction, thereby creating In vacancies (V_{In}) and Ga vacancies (V_{Ga}) [46]. At the KF-CIGSe surface, there is significantly more Na accumulation than at the untreated and RbF-CIGSe surfaces. This could mean formation of more Na_{In} and Na_{Ga} defects in KF-CIGSe than in RbF-CIGSe. Na_{In} defects are known to form shallow acceptor levels [47] and raise the hole concentration. However, since the formation energies of K_{Cu} and Rb_{Cu} defects are lower than that of the Na_{In} defect (Table 1), the former could have been formed in greater quantity and hence resulted in overall reduced acceptor densities (N_A) in both types of alkali treated-CIGSe/CdS interfaces.

(ii) The possibility of Na_{Cd} defects at the KF-CIGSe/CdS interface will have a particularly beneficial effect. Cd vacancies (V_{Cd}^{2-}) that are doubly charged in the buffer layer form deep acceptor levels that result in reduced n-type doping in CdS. Filling up such a vacancy with Na (Na_{Cd}^- defect formation) would lead to increased n-type doping [48]. The Na_{Cd}^- defect then has a lower hole capture cross-section as well as this defect level being shallower than the V_{Cd}^{2-} defect helps in reducing recombination centres at the absorber/buffer interface. Na_{Cd} has a negative defect formation enthalpy (Table 1) and has been shown to be a soluble acceptor in CdS [49]. There could be a possibility of Na diffusion into the CdS layer and forming the beneficial Na_{Cd} defects. Moreover, due to excess of Na at the KF-CIGSe surface, Na diffusion out of CIGSe into CdS is possible at the CBD temperature of ~ 46 °C. Koprek et al. [50] showed ~ 0.2 at. % of Na segregated on the CdS side of a CIGSe/CdS interface using atom probe tomography (APT) that has a very low elemental concentration detection limit in the range of parts per million (ppm). Such low Na concentrations would go undetected with XPS, which could be the case for our studied interfaces.

(iii) It was also observed that for the same conditions of CdS deposition (simultaneous deposition in a common chemical bath) for all the absorbers, the Cd intake of the KF-CIGSe absorber was the highest of all (Figure 4) indicating formation of more Cd_{Cu} defects in this case that are known to form shallow donor levels and thus facilitate type-inversion at the absorber/buffer interface [48], which can improve the heterojunction quality. This higher Cd intake is in agreement with the Cu-enrichment seen in the *near-bulk* region of the KF-CIGSe/CdS interface (Figure 5), thus leaving more Cu vacancies in the *near-surface* region for the incoming Cd atoms to fill them.

3.5 Solar cell device performance evaluation

Table 2 shows the average cell parameters of the devices made from the untreated and alkali-treated CIGSe absorbers made in this work. The devices made from alkali-treated absorbers show significantly better open-circuit voltages (V_{oc}) and slightly better fill factors (FF) and efficiencies (η) than the untreated CIGSe reference device. Among the alkali-treated absorbers, the device made from the KF-CIGSe absorber shows higher V_{oc} , FF and η as compared to the device made from the RbF-CIGSe absorber. This observation is in agreement with the work of Avancini et al. [26] where the best cell for their KF-treated CIGSe device is slightly better than their RbF-treated CIGSe device. Whereas, Jackson et al. [8] showed slightly better η for their devices made from a RbF-treated CIGSe absorber as compared to the ones made from a KF-treated CIGSe absorber. Thus, it can be seen that the performance of KF-treated and RbF-treated CIGSe devices have no dependency on the size of the respective alkali atoms as opposed to what is proposed by Jackson et al. [8].

Table 2 Mean values of cell parameters of the devices (values measured on 3 best cells of each device) made from CIGSe, KF-CIGSe and RbF-CIGSe absorbers.

Devices	J_{sc} (mA cm ⁻²)	V_{oc} (mV)	FF (%)	η (%)
CIGSe	37.4±0.3	585±10	63.3±2.6	14.0±0.9
KF-CIGSe	36.9±0.6	637±5	65.7±2.9	15.4±0.6
RbF-CIGSe	36.3±0.5	617±4	65.0±2.9	14.5±0.7

SCAPS [51] is a one dimensional solar cell simulation program that works on the basis of solving for the classical Poisson's and the continuity equations for charge carriers at a p-n junction. This device simulation section focuses on the conditions under which there could be a FF gain in addition to the V_{oc} gain in resulting devices, a trend of which has been observed in the measured devices in this work. The simulation models consist of a basic p-type CIGSe 1-D structure. Table S6 in SI 9 shows all the SCAPS simulation parameters, i.e. the various layer properties of the model solar cell stack. Since the studied CIGSe absorbers had Na from the soda-lime glass (SLG) substrate, an acceptor doping level of $N_A=1 \times 10^{16}$ cm⁻³ in the CIGSe bulk was considered. For the KF-treated CIGSe device, a CIGSe:K/K-(In,Ga)-Se/CdS model has been considered, which is a 10 nm thick K-(In,Ga)-Se surface layer with $E_g=2.68$ eV (measured optical band-gap of similar compound prepared by Kish et al. [52]) on top of a CIGSe absorber with K incorporated in its bulk with a $[K]/([K]+[Cu])$ (KKC) ratio of 0.37. For the RbF-treated CIGSe device, a similar CIGSe:Rb/Rb-(In,Ga)-Se/CdS model has been considered, which is a 10 nm thick Rb-(In,Ga)-Se surface layer with $E_g=2.00$ eV (measured optical band-gap of similar compound prepared by Huang et al. [53]) on top of a CIGSe absorber with Rb incorporated in its bulk with a $[Rb]/([Rb]+[Cu])$ (RRC) ratio of 0.34. The

resulting device parameters are shown in Table 3. The J_{sc} values in the CIGSe:K/K-(In,Ga)-Se/CdS and the CIGSe:Rb/Rb-(In,Ga)-Se/CdS models have been influenced by the E_g values of the respective K-(In,Ga)-Se and Rb-(In,Ga)-Se secondary phases.

Table 3 Simulated device parameters for the various models.

Device model	J_{sc} (mA/cm ²)	V_{oc} (mV)	FF (%)	η (%)
CIGSe/CdS	31.1	826	75.1	19.3
CIGSe:K/K-(In,Ga)-Se/CdS	30.3	883	81.3	21.8
CIGSe:Rb/Rb-(In,Ga)-Se/CdS	32.4	860	77.0	21.5

From the simulations, the gain in V_{oc} is a direct consequence of the increase in E_g of the CIGSe:K or CIGSe:Rb absorber. From Table 3, it can be seen that the gain in V_{oc} in CIGSe:K/K-(In,Ga)-Se/CdS model device (57 mV) and CIGSe:Rb/Rb-(In,Ga)-Se/CdS model device (34 mV) w.r.t. the reference CIGSe/CdS model device results from a corresponding change in absorber E_g of both alkali-treated absorbers being 0.062 eV for KF-CIGSe and being 0.037 eV for RbF-CIGSe w.r.t. reference CIGSe. An E_g increase of 0.20 eV in the absorber as a result of K incorporation in the Cu-deficient $Cu_5In_9Se_{16}$ has also been predicted theoretically by Xiao et al. [13].

On the other hand, from the discussion of the effect of point defects in the previous section, it has been understood that the alkali treatment may contribute to stronger type-inversion at the absorber/buffer interface. The electron affinity (χ) and the acceptor and donor density values at the interface region influence the extent of type-inversion and this, in turn, influences the FF. The gain in FF is contributed from the type-inversion generated by the point defects at the absorber/buffer interface. Therefore, in the present simulations, considering the K-(In,Ga)-Se and Rb-(In,Ga)-Se layers as the interface regions, and altering the χ and doping concentrations (N_A , N_D) in this region led to improvement in FF, which is also in agreement with the real device results and spectroscopic observations. Spectroscopically, an increase in the χ value is seen as the downward shift of the VBM w.r.t. E_F as a result of both KF and RbF treatment (Figure 8). Absorber VBM shifts away from the Fermi level / VBM downward shift / VBM lowering at the absorber/buffer interface indicates towards increased n-type doping at the interface as compared to the bulk of the absorber which is p-type doped, and hence $p \rightarrow n$ type-inversion. The relation between VBM lowering and type-inversion has also been explored in our previous work [54]. Moreover, N_D in the K-(In,Ga)-Se layer is greater than that in the Rb-(In,Ga)-Se layer, which could be associated with Na_{Cd} and excess Cd_{Cu} defects at the KF-CIGSe/CdS interface. Comparing the N_A values indicates higher acceptor density at the KF-CIGSe/CdS interface that can be associated with the higher amount of Na_{In} and Na_{Ga}

shallow acceptor defects as compared to the RbF-CIGSe/CdS interface. Figure 9 shows the band diagrams of the simulated alkali-treated CIGSe devices (shown in Table 3), highlighting the above mentioned factors leading to type-inversion at the interfaces. Thus from the simulations, we derived that the type-inversion caused by point defects influences the FF and the band gaps of the CIGSe:K and CIGSe:Rb absorber layers influence the V_{oc} of the devices. Hence, both these factors influence device performances. Moreover, it can be said that the presence of a high band gap secondary phase at the CIGSe absorber surface cannot be the only contributing factor for increased conversion efficiencies as was suggested by Handick et al. [55]. In addition, we tried to decipher what factors could have possibly led to our device performance trend (KF treatment slightly better than RbF treatment).

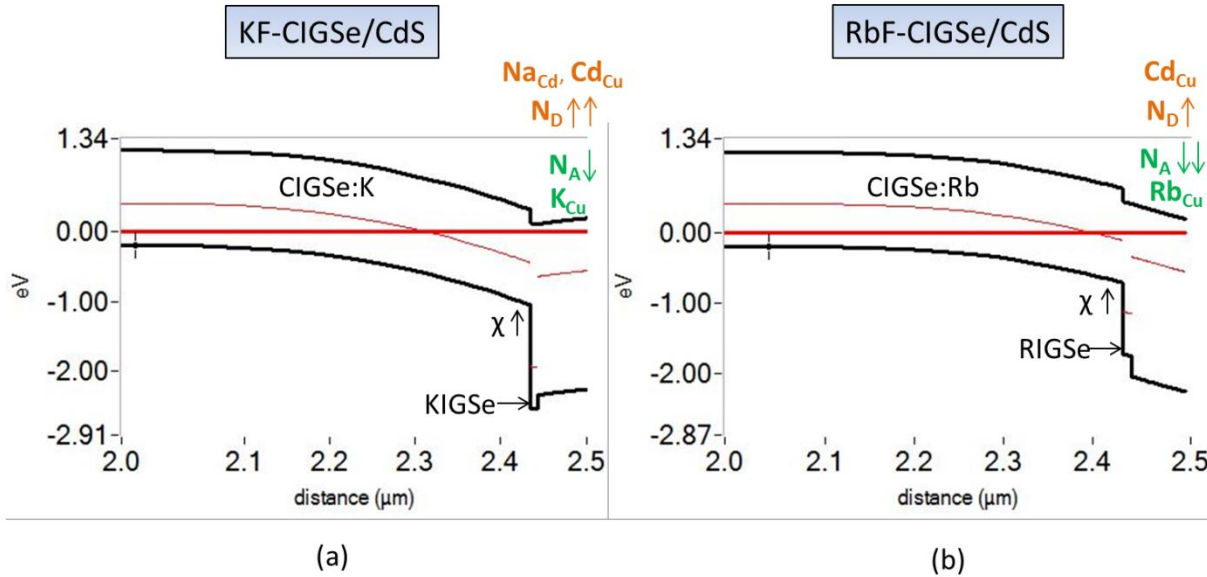


Figure 9 (color online) Band diagrams obtained from SCAPS simulations. Upper and lower levels in black (bold) are E_{CBM} and E_{VBM} , respectively. Intermediate level in red (bold) is E_F . Other intermediate levels in red (light) are the deep defect levels (E_T). The KF-CIGSe/CdS interface shows a strong type-inversion while the RbF-CIGSe/CdS interface shows a tendency towards type-inversion.

A model for the beneficial effect of KF treatment proposed by Lepetit [45] had suggested the presence of an ODC-like surface layer on CIGSe; Cu-reduction by Cu migration into this ODC phase and K replacement of Cu; In-enrichment and GaF_3 formation at the absorber surface. All these absorber surface-related changes are in good agreement with the observations of our study, in terms of the presence of a *near-surface* ODC-like composition; K_{Cu} defect formation and Ga-F and In-F formation at the KF-CIGSe surface. While at the interface with CdS, Lepetit [45] suggested the formation of the compound $CdIn_2(S,Se,OH)_4$ by either Cd replacing K and S replacing Se in $KInSe_2$ or simply a reaction between CdS and In_2Se_3 without the

involvement of K. From the observations gathered in our study, S replacing Se can be supported from the S-Se intermixing observed at the KF-CIGSe/CdS interface. A reaction between CdS and In-O can be supported by the observation that In-O forms at both KF-CIGSe and RbF-CIGSe surfaces. Moreover, this $\text{CdIn}_2(\text{S,Se,OH})_4$ compound has been found to be n-type, which supports the type-inversion model considered in our study.

4. Conclusions

The purpose of this study was two-fold: (i) to compare the similarities and differences in KF and RbF treatments using HAXPES analysis, (ii) to investigate factors that might be responsible for the FF gain due to these treatments in addition to V_{oc} gain using DFT and SCAPS simulations.

We have shown here that the KF treatment led to a better real device performance than the RbF treatment. Both KF and RbF treatments have resulted in some chemical modifications in the absorbers in common such as Cu-poor *near-surface* and Cu, In, Ga-rich *near-bulk* absorber regions; formation of In-O, In-F and Ga-F compounds at the surfaces; and respective alkali-CIGSe related secondary phase formation at the absorber surfaces. Some differences in surface modifications were an ODC-like *near-surface* composition in KF-CIGSe while a highly Cu-poor *near-surface* composition in RbF-CIGSe; and In-F compound formation in higher quantity at the KF-CIGSe surface than at the RbF-CIGSe surface. As for the interfaces, the *near-interface* regions of both alkali-treated CIGSe/CdS interfaces were found to be ODC-like, while the *near-bulk* regions were found to be In, Cd-rich. Greater S-Se intermixing at the KF-CIGSe/CdS interface could indicate towards mixed absorber-buffer related secondary phase formation at the interface.

From DFT calculations and spectroscopic observations, there is an indication that the K_{Cu} , Na_{Cd} and Na_{In} defects are more likely to be formed at the KF-CIGSe/CdS interface; while Rb_{Cu} defects may be formed at the RbF-CIGSe/CdS interface. Moreover, a high Cd intake at the KF-CIGSe/CdS interface would mean more Cd_{Cu} defect formation. The combined effect of the lowering of N_{A} due to K_{Cu} defects and the increase of N_{D} due to Na_{Cd} and Cd_{Cu} defects at the KF-CIGSe/CdS interface might have resulted in a stronger type-inversion that led to an enhanced FF in the KF-CIGSe real device along with a V_{oc} gain. A similar effect due to the presence of Rb_{Cu} and Cd_{Cu} defects at the RbF-CIGSe/CdS interface may have resulted in a higher FF in the RbF-CIGSe real device in comparison to the untreated CIGSe real device, in addition to a V_{oc} gain. Moreover, VBM shifts of +0.52 eV and +0.38 eV away from the Fermi level at the KF-CIGSe/CdS and RbF-CIGSe/CdS interfaces, respectively, may indicate towards an increase in χ after CdS deposition that could further enhance the interfacial type-inversion and increase the FF in the devices.

In general, it can be suggested that the controlled tuning of KKC or [Rb]/([Rb]+[Cu]) (RRC) ratios alone can improve V_{oc} of CIGSe-based devices. This means that the V_{oc} could be significantly influenced by bulk recombination alone. Therefore, $Cu_{1-x}K_xIn_{1-y}Ga_ySe_2$ and $Cu_{1-x}Rb_xIn_{1-y}Ga_ySe_2$ alloys as absorbers could be promising candidates to obtain high efficiency solar cells provided they maintain high absorption coefficients similar to CIGSe absorbers. On the other hand, among other factors, the FF gain may be influenced significantly by interface recombination, in terms of the extent of type-inversion. Increased χ and N_D at the absorber/buffer interface have been found to be two crucial factors influencing the FF. For further understanding of interfacial defects that might influence type-inversion, diffusion studies of Na from CIGSe into CdS and Cd from CdS into CIGSe would be relevant.

Acknowledgements

Dr. Roberto F. Duarte is acknowledged for his technical support at the HIKE beamline in BESSY II and Dr. Bünyamin Ümsür is acknowledged for lending beamtime. I. Majumdar thanks her doctoral funding agencies Erasmus Mundus, FAZIT Stiftung and HZB PVcomB. Michael Klupsch (PVcomB, HZB) is acknowledged for introduction to SCAPS simulations. I. Majumdar also thanks Prof. Paul Fumagalli and Dr. Ralph Püttner (FU Berlin, FB Physik) for error considerations and Auger spectra analysis related discussions and Prof. Dr. Martha Ch. Lux-Steiner (FU Berlin, FB Physik), Dr. Christian A. Kaufmann and Dr. Tobias Bertram (PVcomB, HZB) for suggestions for improvement in the manuscript. S. K. Sahoo, T. D. Kühne and H. Mirhosseini acknowledge financial support from the German *Bundesministerium für Wirtschaft und Energie (BMWi)* for the speedCIGS project (0324095C). The authors gratefully acknowledge the Gauss Centre for Supercomputing e.V. (www.gauss-centre.eu) for funding this project (application no-13178) by providing computing time through the John von Neumann Institute for Computing (NIC) on the GCS Supercomputer JUWELS at Jülich Supercomputing Centre (JSC). The generous allocation of computing time by the Paderborn Center for Parallel Computing (PC2) on OCuLUS and the FPGA-based supercomputer NOCTUA is kindly acknowledged.

References

- [1] J. Ramanujam, U. P. Singh, Copper indium gallium selenide based solar cells - a review, *Energy Environ. Sci.*, 10 (6) (2017) 1306-1319.
- [2] T. M. Friedlmeier, P. Jackson, A. Bauer, D. Hariskos, O. Kiowski, R. Menner, R. Wuerz, M. Powalla, High-efficiency $Cu(In,Ga)Se_2$ solar cells, *Thin Solid Films*, 633 (2017) 13-17.

- [3] A. Chirila, P. Reinhard, F. Pianezzi, P. Bloesch, A. R. Uhl, C. Fella, L. Kranz, D. Keller, C. Gretener, H. Hagendorfer, D. Jaeger, R. Erni, S. Nishiwaki, S. Buecheler, A. N. Tiwari, Potassium-induced surface modification of Cu(In,Ga)Se₂ thin films for high-efficiency solar cells, *Nat. Mater.*, 12 (12) (2013) 1107-1111.
- [4] P. Reinhard, B. Bissig, F. Pianezzi, E. Avancini, H. Hagendorfer, D. Keller, P. Fuchs, M. Dobeli, C. Vigo, P. Crivelli, S. Nishiwaki, S. Buecheler, A. N. Tiwari, Postdeposition treatments of Cu(In,Ga)Se₂ absorbers for high efficiency thin film solar cells, *Chem. Mater.*, 27 (16) (2015) 5755-5764.
- [5] C. P. Muzzillo, Review of grain interior, grain boundary, and interface effects of K in CIGS solar cells: Mechanisms for performance enhancement, *Sol. Energy Mater. Sol. Cells*, 172 (2017) 18-24.
- [6] I. Majumdar, V. Parvan, D. Greiner, C. A. Kaufmann, M. Ch. Lux-Steiner, R. Schlatmann, and I. Lauermann, Investigation of KF-treatment induced surface modifications of Cu(In,Ga)Se₂ absorbers and their correlation with device performance, in: *Proceedings of the 33rd European Photovoltaic Solar Energy Conference and Exhibition*, Amsterdam, The Netherlands, 2017, 1127-1132.
- [7] T. Kodalle, M. D. Heinemann, D. Greiner, H. A. Yetkin, M. Klupsch, C. Li, P. A. van Aken, I. Lauermann, R. Schlatmann, C. A. Kaufmann, Elucidating the mechanism of an RbF post deposition treatment in CIGS thin film solar cells, *Sol. RRL*, 2 (2018) 1800156.
- [8] P. Jackson, R. Wuerz, D. Hariskos, E. Lotter, W. Witte, M. Powalla, Effects of heavy alkali elements in Cu(In,Ga)Se₂ solar cells with efficiencies up to 22.6%, *Phys. Status Solidi RRL*, 10 (8) (2016) 583-586.
- [9] Solar Frontier, http://www.solar-frontier.com/eng/news/2019/0117_press.html.
- [10] M. Malitckaya, H. P. Komsa, V. Havu, M. J. Puska, Effect of alkali metal atom doping on the CuInSe₂-based solar cell absorber, *J. Phys. Chem. C*, 121 (29) (2017) 15516-15528.
- [11] E. Ghorbani, J. Kiss, H. Mirhosseini, G. Roma, M. Schmidt, J. Windeln, T. D. Kiihne, C. Felser, *J. Phys. Chem. C*, Hybrid-functional calculations on the incorporation of Na and K impurities into the CuInSe₂ and CuIn₅Se₈ solar-cell materials, 119 (45) (2015) 25197-25203.
- [12] Y. Hinuma, F. Oba, Y. Kumagai, I. Tanaka, Band offsets of CuInSe₂/CdS and CuInSe₂/ZnS (110) interfaces: A hybrid density functional theory study, *Phys. Rev. B: Condens. Matter Mater. Phys.*, 88 (3) (2013) 035305.
- [13] H. Xiao, W. A. Goddard, Predicted roles of defects on band offsets and energetics at CIGS (Cu(In,Ga)Se₂/CdS) solar cell interfaces and implications for improving performance, *J. Chem. Phys.*, 141 (9) (2014) 094701.
- [14] T. Fu-Ling, L. Ran, X. Hong-Tao, L. Wen-Jiang, F. Yu-Dong, R. Zhi-Yuan, H. Min, Lattice structures and electronic properties of CIGS/CdS interface: First-principles calculations, *Chin. Phys. B*, 23 (2014) 077301.

- [15] A. J. Nelson, S. Gebhard, A. Rockett, E. Colavita, M. Engelhardt, H. Hochst, Synchrotron radiation photoemission study of CdS/CuInSe₂ heterojunction formation, *Phys. Rev. B: Condens. Matter Mater. Phys.*, 42 (12) (1990) 7518-7523.
- [16] C. Heske, D. Eich, R. Fink, E. Umbach, T. van Buuren, C. Bostedt, L. J. Terminello, S. Kakar, M. M. Grush, T. A. Callcott, F. J. Himpsel, D. L. Ederer, R. C. C. Perera, W. Riedl, F. Karg, Observation of intermixing at the buried CdS/Cu(In,Ga)Se₂ thin film solar cell heterojunction, *Appl. Phys. Lett.*, 74 (10) (1999) 1451-1453.
- [17] T. Nakada, A. Kunioka, Direct evidence of Cd diffusion into Cu(In,Ga)Se₂ thin films during chemical-bath deposition process of CdS films, *Appl. Phys. Lett.*, 74 (17) (1999) 2444-2446.
- [18] M. Morkel, L. Weinhardt, B. Lohmuller, C. Heske, E. Umbach, W. Riedl, S. Zweigart, F. Karg, Flat conduction-band alignment at the CdS/CuInSe₂ thin-film solar-cell heterojunction, *Appl. Phys. Lett.*, 79 (27) (2001) 4482-4484.
- [19] T. Schulmeyer, R. Hunger, A. Klein, W. Jaegermann, S. Niki, Photoemission study and band alignment of the CuInSe₂(001)/CdS heterojunction, *Appl. Phys. Lett.*, 84 (16) (2004) 3067-3069.
- [20] S. M. Park, T. G. Kim, Y. D. Chung, D. H. Cho, J. Kim, K. J. Kim, Y. Yi, J. W. Kim, Junction formation at the interface of CdS/CuIn_xGa_(1-x)Se₂, *J. Phys. D: Appl. Phys.*, 47 (34) (2014) 345302.
- [21] D. Hauschild, D. Kreikemeyer-Lorenzo, P. Jackson, T. M. Friedlmeier, D. Hariskos, F. Reiner, M. Powalla, C. Heske, L. Weinhardt, Impact of a RbF postdeposition treatment on the electronic structure of the CdS/Cu(In,Ga)Se₂ heterojunction in high-efficiency thin-film solar cells, *ACS Energy Lett.*, 2 (10) (2017) 2383-2387.
- [22] N. Nicoara, T. Kunze, P. Jackson, D. Hariskos, R. F. Duarte, R. G. Wilks, W. Witte, M. Bar, S. Sadewasser, Evidence for chemical and electronic nonuniformities in the formation of the interface of RbF-treated Cu(In,Ga)Se₂ with CdS, *ACS Appl. Mater. Interfaces*, 9 (50) (2017) 44173-44180.
- [23] P. M. P. Salome, R. Ribeiro-Andrade, J. P. Teixeira, J. Keller, T. Torndahl, N. Nicoara, M. Edoff, J. C. Gonzalez, J. P. Leitao, S. Sadewasser, Cd and Cu interdiffusion in Cu(In,Ga)Se₂/CdS heterointerfaces, *IEEE Journal of Photovoltaics*, 7 (3) (2017) 858-863.
- [24] F. Werner, F. Babbe, J. Burkhart, C. Spindler, H. Elanzeery, S. Siebentritt, Interdiffusion and doping gradients at the buffer/absorber interface in thin-film solar cells, *ACS Appl. Mater. Interfaces*, 10 (34) (2018) 28553-28565.
- [25] P. Yang, R. G. Wilks, W. Yang, M. Bär, Interface formation between CdS and alkali post-deposition treated Cu(In,Ga)Se₂ thin-film solar cell absorbers - Key to understanding the efficiency gain, *ACS Appl. Mater. Interfaces*, 12(5) (2020) 6688-6698.

- [26] X. Q. He, T. Paulauskas, P. Ercius, J. Varley, J. Bailey, G. Zapalac, D. Poplaskyy, N. Mackie, A. Bayman, D. Spaulding, R. Klie, V. Lordi, A. Rockett, Cd doping at PVD-CdS/Cu(In,Ga)Se₂ heterojunctions, *Sol. Energy Mater. Sol. Cells*, 164 (2017) 128-134.
- [27] R. O. Jones, Density functional theory: Its origins, rise to prominence, and future, *Rev. Mod. Phys.*, 87 (3) (2015) 897-923.
- [28] C. A. Kaufmann, A. Neisser, R. Klenk, R. Scheer, Transfer of Cu(In,Ga)Se₂ thin film solar cells to flexible substrates using an in situ process control, *Thin Solid Films*, 480 (2005) 515-519.
- [29] M. D. Heinemann, R. Mainz, F. Osterle, H. Rodriguez-Alvarez, D. Greiner, C. A. Kaufmann, T. Unold, Evolution of opto-electronic properties during film formation of complex semiconductors, *Sci. Rep.*, 7 (2017) 45463.
- [30] MBE Komponenten, Dr. Eberl, <https://www.mbe-komponenten.de/products/pdf/data-sheet-wez.pdf>.
- [31] M. Gorgoi, S. Svensson, F. Schafers, G. Ohrwall, M. Mertin, P. Bressler, O. Karis, H. Siegbahn, A. Sandell, H. Rensmo, W. Doherty, C. Jung, W. Braun, W. Eberhardt, The high kinetic energy photoelectron spectroscopy facility at BESSY progress and first results, *Nucl. Instrum. Methods Phys. Res., Sect. A*, 601 (1-2) (2009) 48-53.
- [32] F. Schafers, The crystal monochromator beamline KMC-1 at BESSY II, *Journal of large-scale research facilities*, 2 (2016) A96.
- [33] M. B. Trzhaskovskaya, V. I. Nefedov, V. G. Yarzhemsky, Photoelectron angular distribution parameters for elements Z=1 to Z=54 in the photoelectron energy range 100-5000 eV, *At. Data Nucl. Data Tables*, 77 (1) (2001) 97-159.
- [34] A. Baldereschi, S. Baroni, R. Resta, Band offsets in lattice-matched heterojunctions - A model and 1st-principles calculations for GaAs/AlAs, *Phys. Rev. Lett.*, 61 (6) (1988) 734-737.
- [35] E. Avancini, R. Carron, T. P. Weiss, C. Andres, M. Burki, C. Schreiner, R. Figi, Y. E. Romanyuk, S. Buecheler, A. N. Tiwari, Effects of rubidium fluoride and potassium fluoride postdeposition treatments on Cu(In,Ga)Se₂ thin films and solar cell performance, *Chem. Mater.*, 29 (22) (2017) 9695-9704.
- [36] P. Jackson, D. Hariskos, R. Wuerz, W. Wischmann, M. Powalla, Compositional investigation of potassium doped Cu(In,Ga)Se₂ solar cells with efficiencies up to 20.8%, *Phys. Status Solidi RRL*, 8 (3) (2014) 219-222.
- [37] D. Briggs, M. P. Seah, *Practical Surface Analysis by Auger and X-ray Photoelectron Spectroscopy*, Wiley, Chichester, 1983.
- [38] NIST X-ray Photoelectron Spectroscopy Database, <https://srdata.nist.gov/xps>.
- [39] B. Tell, J. L. Shay, H. M. Kasper, Electrical Properties, Optical properties, and band structure of CuGaS₂ and CuInS₂, *Phys. Rev. B: Condens. Matter Mater. Phys.*, 4 (8) (1971) 2463.

- [40] I. Majumdar, B. Uemsuer, B. Chacko, D. Greiner, M. Ch. Lux-Steiner, R. Schlatmann, I. Lauermann, Surface modifications of Na and K metal incorporated Cu(In,Ga)Se₂ absorbers investigated by synchrotron-based spectroscopies, *Phys. Status Solidi C*, 14 (10) (2017) 1700167.
- [41] T. Kodalle, R. K. M. Raghupathy, T. Bertram, N. Maticiuc, H. A. Yetkin, R. Gunder, R. Schlatmann, T. D. Kuhne, C. A. Kaufmann, H. Mirhosseini, Properties of co-evaporated RbInSe₂ thin films, *Phys. Status Solidi RRL*, 13 (3) (2019) 1800564.
- [42] T. Lepetit, Influence of KF post deposition treatment on the polycrystalline Cu(In,Ga)Se₂/CdS heterojunction formation for photovoltaic application, Ph.D thesis, University of Nantes, France, 2015.
- [43] M. Ruckh, D. Schmid, M. Kaiser, R. Schaffler, T. Walter, H. W. Schock, Influence of substrates on the electrical properties of Cu(In,Ga)Se₂ thin films, in: Conference Record of the 24th IEEE Photovoltaic Specialists Conference, Vols. I and II, Hawaii, USA, 1994, 156-159.
- [44] B. M. Keyes, F. Hasoon, P. Dipppo, A. Balcioglu, F. Abulfotuh, Influence of Na on the electro-optical properties of Cu(In,Ga)Se₂, in: Conference Record of the 26th IEEE Photovoltaic Specialists Conference, Anaheim, USA, 1997, 479-482.
- [45] Z. K. Yuan, S. Y. Chen, Y. Xie, J. S. Park, H. J. Xiang, X. G. Gong, S. H. Wei, Na-diffusion enhanced p-type conductivity in Cu(In, Ga)Se₂: A new mechanism for efficient doping in semiconductors, *Adv. Energy Mater*, 6 (24) (2016) 1601191.
- [46] J. Bekaert, R. Saniz, B. Partoens, D. Lamoen, Native point defects in CuIn_(1-x)Ga_xSe₂: hybrid density functional calculations predict the origin of p- and n-type conductivity, *Phys. Chem. Chem. Phys.*, 16 (40) (2014) 22299-22308.
- [47] S. H. Wei, S. B. Zhang, A. Zunger, Effects of Na on the electrical and structural properties of CuInSe₂, *J. Appl. Phys. (Melville, NY, U.S.)*, 85 (10) (1999) 7214-7218.
- [48] J. B. Varley, V. Lordi, Intermixing at the absorber-buffer layer interface in thin-film solar cells: The electronic effects of point defects in Cu(In,Ga)(Se,S)₂ and Cu₂ZnSn(Se,S)₄ devices, *J. Appl. Phys. (Melville, NY, U.S.)*, 116 (6) (2014) 063505.
- [49] C. H. Henry, K. Nassau, J. W. Shiever, Optical studies of shallow acceptors in CdS and CdSe, *Phys. Rev. B: Condens. Matter Mater. Phys.*, 4 (8) (1971) 2453.
- [50] A. Koprek, O. Cojocaru-Miredin, R. Wuerz, C. Freysoldt, B. Gault, D. Raabe, Cd and impurity redistribution at the CdS/CIGS interface after annealing of CIGS-based solar cells resolved by atom probe tomography, *IEEE Journal of Photovoltaics*, 7 (1) (2017) 313-321.
- [51] M. Burgelman, P. Nollet, S. Degraeve, Modelling polycrystalline semiconductor solar cells, *Thin Solid Films*, 361 (2000) 527-532.

- [52] Z. Z. Kish, V. B. Lazarev, E. Y. Peresh, E. E. Semrad, Compounds in the system $\text{In}_2\text{Se}_3\text{-K}_2\text{Se}$, *Inorg. Mater.*, 24 (10) (1988) 1371-1374.
- [53] F. Q. Huang, B. Deng, D. E. Ellis, J. A. Ibers, Preparation, structures, and band gaps of RbInS_2 and RbInSe_2 , *J. Solid State Chem.*, 178 (6) (2005) 2128-2132.
- [54] I. Majumdar, V. Parvan, D. Greiner, R. Schlatmann, I. Lauermann, Effect of Na from soda-lime glass substrate and as post-deposition on Cu(In,Ga)Se_2 absorbers: A photoelectron spectroscopy study in ultra-high vacuum, *Appl. Surf. Sci.*, 514 (2020) 145941.
- [55] E. Handick, P. Reinhard, J. H. Alsmeier, L. Kohler, F. Pianezzi, S. Krause, M. Gorgoi, E. Ikenaga, N. Koch, R. G. Wilks, S. Buecheler, A. N. Tiwari, M. Baer, Potassium postdeposition treatment-induced band gap widening at Cu(In,Ga)Se_2 surfaces - Reason for performance leap?, *ACS Appl. Mater. Interfaces*, 7 (49) (2015) 27414-27420.